Earth Syst. Sci. Data Discuss., 8, 317–344, 2015
www.earth-syst-sci-data-discuss.net/8/317/2015/
doi:10.5194/essdd-8-317-2015

Open Access Earth System Science Data Discussions

Perceived temperature in the course of climate change: an analysis of global heat index from 1979–2013

D. Lee[1] **and T. Brenner**[2]

[1]German Meteorological Service, Frankfurterstr. 135, 63067 Offenbach, Germany
[2]University of Marburg, Deutschhausstr. 10, 35032 Marburg, Germany

Received: 27 December 2014 – Accepted: 4 March 2015 – Published: 19 March 2015

Correspondence to: D. Lee (daniel.lee@dwd.de)

Published by Copernicus Publications.

Abstract

The increase in global mean temperatures resulting from climate change has wide reaching consequences for the earth's ecosystems and other natural systems. Many studies have been devoted to evaluating the distribution and effects of these changes. We go a step further and evaluate global changes to the heat index, a measure of temperature as perceived by humans. Heat index, which is computed from temperature and relative humidity, is more important than temperature for the health of humans and other animals. Even in cases where the heat index does not reach dangerous levels from a health perspective, it has been shown to be an important factor in worker productivity and thus in economic productivity.

We compute heat index from dewpoint temperature and absolute temperature 2 m above ground from the ERA-Interim reanalysis dataset for the years 1979–2013. The data is provided aggregated to daily minima, means and maxima (doi:10.1594/PANGAEA.841057). Furthermore, the data is temporally aggregated to monthly and yearly values and spatially aggregated to the level of countries after being weighted by population density in order to demonstrate its usefulness for the analysis of its impact on human health and productivity. The resulting data deliver insights into the spatiotemporal development of near-ground heat index during the course of the past 3 decades. It is shown that the impact of changing heat index is unevenly distributed through space and time, affecting some areas differently than others. The likelihood of dangerous heat index events has increased globally. Also, heat index climate groups that would formerly be expected closer to the tropics have spread latitudinally to include areas closer to the poles. The data can serve in future studies as a basis for evaluating and understanding the evolution of heat index in the course of climate change, as well as its impact on human health and productivity.

ESSDD
8, 317–344, 2015

1 Introduction

The essential cause of climate change is the additional entrapment of thermal energy in the earth's many natural systems through climate gases. The speed at which this is occuring is, on climatological and geological time scales, extremely rapid, often requiring faster adaptation than would be expected under normal circumstances (IPCC, 2014).

This additional heat energy has manifold consequences on multiple systems, many of them indirect. All of them, in one way or another, affect humans. For example, additional heat modifies the earth's water household, reducing agricultural yields and in this way affecting human health and well-being (Calzadilla et al., 2010). More directly, additional heat load requires workers to work more slowly and take more breaks, resulting in measurably lower regional productivity (Kjellstrom et al., 2009). Extreme heat can have serious health consequences, especially among the sick and the elderly. In 2003, more than 10 000 deaths in a single month in France were directly attributed to a heat wave (Poumadère et al., 2005). This list could easily be expanded to include other events and regions, and several studies have shown not only that extreme heat events can be expected with higher frequency, but also that heat load in general should increase in the future (Beniston, 2004; Schär et al., 2004; IPCC, 2014).

Large numbers of studies have been devoted to analyzing the effects of climate change on global temperatures and their distribution in space and time (e.g., Vose et al., 2005; Diffenbaugh and Ashfaq, 2010; Diffenbaugh and Scherer, 2011; Alexander and Arblaster, 2009; Meehl et al., 2009; Smith et al., 2005; Sherwood et al., 2008). It has also been shown that changes in the earth's thermal energy household lead to changes in its water cycle. Those changes that affect both the flow of latent and sensible heat are thus the most directly relevant for human physiology. The body rids itself of thermal energy partially through the evaporation of sweat. This process becomes less efficient with higher humidity. For this reason, most metrics that measure heat exposure take both temperature and humidity into account. The wet bulb globe temperature

ESSDD
8, 317–344, 2015

(WBGT), which incorporates the effect of temperature, humidity, wind speed and radiation into a metric for heat stress in humans, has been used in several health and safety standards to measure heat loads and help prevent heat illnesses (e.g., International Organization for Standardization, 2010; National Institute for Occupational Safety and Health, 1986).

Although WBGT is an accurate metric for heat load on humans, the number of variables needed to compute it hinder its use in regional or global scale applications. In the field of meteorology, a much more common metric is apparent temperature, measured using the heat index (Anderson et al., 2013). This metric has seen wider adoption in the health and meteorological communities due to its dependence solely on humidity and temperature (e.g., Perry et al., 2011; Kysely and Kim, 2009; El Morjani et al., 2007; Burkart et al., 2011; Basara et al., 2010).

We present a new data set of globally gridded heat index values computed from reanalysis results for the years 1979–2013. These values are aggregated on several temporal and spatial scales. The data are analyzed and presented in the context of global climate change and its direct effects on human health. We describe the effects of climate change on the global distribution of heat index and investigate these effects for different countries by measuring the change between 2 reference periods in the study's time frame. The data are available for further use by the scientific community (Lee, 2014). It is our hope that these data can serve as a basis for further studies to evaluate and understand changes in heat index over the course of climate change and how these changes impact different areas of human society.

2 Material and methods

2.1 Computing gridded heat index

Observation data over climate-scale time periods are distributed sparsely through space. High quality, consistent data measured at the same place over long periods

ESSDD
8, 317–344, 2015

of time is even rarer. For this reason, we decided to use reanalysis data in order to create our dataset.

Reanalysis data is not an equivalent to observation data and should be used carefully (Thorne and Vose, 2010). Nonetheless, for a study such as ours, reanalysis data can be the most appropriate choice. A priority was to produce spatially and temporally continuous data of a consistent quality for the entire globe over a long period of time. Especially high spatiotemporal resolution was not required. On the other hand, as many high quality observations should be incorporated into the data as possible, without introducing anomalous signals e.g. through changes in observation techniques, shifts in observation locations, etc.

The ERA-Interim reanalysis by the Europe Centre for Medium-Range Weather Forecasts (ECMWF) was considered optimal for this task. It uses the same data assimilation system and dynamic modeling core over a long period of time – from 1979 extended up until the present. The model used to produce the reanalysis, the ECMWF's Integrated Forecast System (IFS), uses 3 fully coupled components for atmosphere, land surface and ocean waves. This improves accuracy especially for areas surrounded mostly by ocean. Because the model is used to produce a reanalysis, which does not have to be published in a time critical fashion, observations from all over the globe can be assimilated, even if they are only available after a normal forecast model's cutoff time. These observations can be quality controlled before being assimilated into the model. Using a model rather than e.g. a simpler interpolation approach makes it possible for the model to propagate information obtained through observations through variable domains, space and time (Dee et al., 2011). All of these criteria made ERA-Interim an intuitive choice as a basis for our study.

The ERA-Interim reanalysis uses 4 assimilation cycles per day, at 00:00, 06:00, 12:00 and 18:00 UTC. The data is produced on a reduced Gaussian grid with approximately uniform spacing for surface fields of 79 km (Berrisford et al., 2009). We used all analyses from the entire available time period of 1979–2013. Forecasts were not used, as we were interested in the highest possible accuracy without the necessity of a high

ESSDD
8, 317–344, 2015

temporal resolution. The data was downloaded after interpolation from the Gaussian onto a regular 0.75° × 0.75° latitude-longitude grid to ease processing in various GIS. Two variables were downloaded: air temperature and dewpoint temperature, both in 2 m height above ground.

Heat index has been computed using a variety of algorithms in different studies. We chose the currently operational method used by the US National Weather Service (2014a), which was developed by Rothfusz (1990) based on work by Steadman (1979), because it is used widely in the operational production of weather warnings in real-life situations and demonstrates the best agreement among heat index algorithms with the original equations by Steadman (Anderson et al., 2013).

This algorithm requires relative humidity and temperature in °F at 2 m above ground as input. Therefore, the input data had to be converted into the required units. This, as well as all subsequent steps described in this section, was done using GRASS GIS (GRASS Development Team, 2012). Of the many possible ways to compute relative humidity from dewpoint temperature (see e.g. Lawrence, 2005), we decided to follow the methodology of the National Weather Service (Murphy, 2006) for the sake of consistency with the method of computing heat index. It is computed as follows:

$$\mathrm{RH} = \left(\frac{112 - 0.1T + T\mathrm{d}}{112 + 0.9T}\right)^8 \quad (1)$$

with RH as relative humidity, T as temperature in °C and Td as dewpoint temperature in °C.

Heat index was computed using an algorithm beginning with a simple approximation:

$$\mathrm{HI} = \frac{T + 61.0 + ((T - 68.0) \cdot 1.2) + (\mathrm{RH} \cdot 0.094)}{2} \quad (2)$$

where HI is heat index in °F, T the temperature in °F and RH the relative humidity.

ESSDD
8, 317–344, 2015

If HI is $< 80\,^{\circ}\mathrm{F}$, this approximation is kept as the final result. Otherwise, it must be computed with a more precise regression:

$$\begin{aligned}\mathrm{HI} = &-42.379 + 2.04901523 \cdot T + 10.14333127 \cdot \mathrm{RH} - 0.22475541 \cdot T \cdot \mathrm{RH} \\ &- 0.00683783 \cdot T^2 - 0.05481717 \cdot \mathrm{RH}^2 + 0.00122874 \cdot T^2 \cdot \mathrm{RH} \\ &+ 0.00085282 \cdot T \cdot \mathrm{RH}^2 - 0.00000199 \cdot T^2 \cdot \mathrm{RH}^2 \end{aligned} \tag{3}$$

An adjustment is added to the result of the last equation dependent on the original inputs in order to obtain the final result:

$$\text{adjustment} = \begin{cases} \frac{13-\mathrm{RH}}{4} \cdot \sqrt{\frac{17-|T-95|}{17}} & \text{if RH} < 0.13 \text{ and } 80 < T < 112 \\ \frac{\mathrm{RH}-85}{10} \cdot \frac{87-T}{5} & \text{if RH} > 0.85 \text{ and } 80 < T < 87 \\ 0 & \text{else} \end{cases} \tag{4}$$

The heat index was calculated for each grid point in each time step we used from the reanalysis. Subsequently, the data were aggregated to daily levels. Although heat index was computed for all 4 assimilations of each day, we used temporally aggregated values in order to produce daily metrics that allowed comparison of global values without forcing the user to account for different time zones. For each day, the 4 assimilations were combined in order to produce gridded daily minima, means and maxima. We considered this a good approximation of the nighttime heat index, which represents the daily minimum in most cases, the actual local mean heat index over the course of the day and the daily midday heat index, which is the maximum in most cases. In addition to producing these daily aggregates, the daily metrics were aggregated to monthly and yearly temporal levels. Finally, the monthly metrics were combined to produce typical heat index years for the periods 1979–1999 and 2000–2013 in order to allow climatological comparison of the two periods. Although neither of these periods represents a typical 30 year climate period, this was considered a good compromise which preserved the division between the typical climate periods of 1970–1999 and 2000–2029

ESSDD
8, 317–344, 2015

while splitting the data into temporal chunks of similar lengths. The resultant data was compared using the raster analysis package for the statistical software R (Hijmans, 2014; R Core Team, 2014).

2.2 Initial analysis: country-based population weighted aggregation

The primary reason that heat index is so relevant in the context of climate change is its direct and indirect effects on human health and the anthropogenic systems connected to it. This motivated us to not only aggregate the global data temporally, but also spatially to the level of countries. Particularly the heat index in populated areas was considered relevant, as dangerous heat exposure in areas where no people are affected is at most tangentially connected to human well-being. High-quality, gridded and spatially continuous data on human population was necessary in order to weight the computed heat index by the population in the relevant grid cells, and thus by its impact on human systems.

The Global Rural-Urban Mapping Project (GRUMP) (CIESIN – Columbia University; IFPRI; The World Bank; CIAT, 2011) contains high-quality gridded population data. The dataset consists of estimates of human population for the years 1990, 1995 and 2000 on a 30 arc-second grid (meaning a horizontal resolution of approximately 1 km) for the entire globe.

GRUMP is based on work originally done for the Gridded Population of the World (GPW) dataset (CIESIN – Columbia University; IFPRI; The World Bank; CIAT, 2004), which was produced by resampling census and survey data for administrative units onto a regular grid. The population was temporally interpolated between sampling points to the above-mentioned snapshot years. GRUMP refined the GPW data by identifying urban areas with the help of administrative data and night time satellite imagery. Population was then redistributed inside administrative areas to the respective urban and rural areas in order to match the proportion of urban-rural population described by data from the United Nations (Balk et al., 2010).

ESSDD
8, 317–344, 2015

We had the highest confidence in the estimates refined using satellite data for 1990 because we considered it to be generally closer to the original input data. Because of the large number of changes in administrative boundaries and population distribution in the years after the dissolution of the Soviet Union in 1991, the authors of GRUMP were often forced to combine heterogeneous data sources into their results (Balk and Yetman, 2004). Although this was done with a high degree of care and in-depth knowledge of each individual case, the uncertainties that this produced prompted us to consider using the estimates from 1990 to be the best compromise between quality, consistency and the required accuracy for our analyses.

For the sake of consistency, we aggregated the population data into current political boundaries (Patterson and Kelso, 2014), rather than adjusting the data to accommodate the modification, addition or dissolution of national borders over time. Therefore, all statements about changes in the climate of given countries in this study should be interpreted as referring to the geographic areas currently officially occupied by the country in question, rather than the possibly dynamic geographic area occupied by the country over the study period.

Our first step was to rasterize the areas covered by each country onto the same coordinate system as the GRUMP data. This made it possible to discretely sum the population inside each country according to the GRUMP estimates. Per-grid point population weights were produced by calculating the proportion of population within that country that were located within the grid point in question, as follows:

$$p_{\text{weight}} = \frac{p_{\text{count}}}{p_{\text{total}}} \tag{5}$$

where p_{weight} is the cell's population weight inside the country, p_{total} the country's total population and p_{count} the population count for the grid point in question.

The per-country weighted mean heat index was then computed as follows:

$$\text{HI}_{\text{weight}} = \sum p_{\text{weight}} \cdot \text{HI} \tag{6}$$

ESSDD
8, 317–344, 2015

Weighted means were produced for each country with available data and each temporal aggregation level, as outlined in Sect. 2.1.

Subsequently, the population weighted monthly minima, means and maxima per country were used to classify each country into heat index climatology clusters using the statistical software R (R Core Team, 2014). As a first step, the appropriate number of clusters was determined by iterative *k* means clustering (Hartigan and Wong, 1979). For each number of clusters, the sum of squared distance between points in each cluster was examined in order to determine the point at which additional clusters no longer produced useful information (Everitt and Hothorn, 2010, p. 251). Afterwards, the clusters each country was sorted into in each reference period were compared.

3 Results and discussion

The resulting data was visualized for analysis using ggplot2 (Wickham, 2009).

3.1 Global heat index

Figure 1 shows the heat index metrics for the entire globe on a typical day in summer on the Northern Hemisphere. Dangerous heat index levels can be seen both in the daytime maximum, as well as during the night in hot, moist regions near the equator. The diurnal cycle is especially high for hot and moist regions, high for dry areas in which the temperature fluctuates highly in the course of the diurnal cycle, and low in drier areas with relatively small diurnal temperature cycles. It should be noted that the heat index, which was created for the purpose of measuring physiological stress due to high heat loads, is not adapted for measuring stress due to low temperatures. Also, because the heat index was developed in order to measure physiological danger to humans, above a certain level it is oversaturated, so that no additional information can be gained from it. For this reason, we rounded extreme heat index values into the range of 40–140 °F in all subsequent visualizations. This corresponds with the lower

ESSDD
8, 317–344, 2015

bounds of the heat index equation (Anderson et al., 2013) and the rough upper bounds of danger levels used to classify heat index (National Weather Service, 2014b).

The data shows much the same pattern when aggregated to the same metrics for entire years in each reference period (Fig. 2). In both reference periods, extremely high heat index values can occur over most of the earth's land masses. The mean heat index values increase between reference periods to a small degree, as do the minimum heat index values. The spatial distribution remains similar in both reference periods – the highest heat index values occur near the equator over the Gulf of Mexico, the Indian Ocean and the western Pacific, where both temperature and air moisture is high. The equatorial belt of high heat index values is roughly evenly distributed on both sides of the equator, as the metrics are aggregated over both north and south summer. The transport of heat and air moisture toward Europe by the Gulf Stream is also visible.

The change between both reference periods is shown more clearly in Fig. 3. The maximum heat index shows large changes in both directions for individual cells. This is due to the fact that the maximum heat index for each entire reference period stems from single, significant events that are highly specific in both time and space. This causes spatial shifts in the occurrence of extreme heat index events to produce large deviances between reference periods, similar to the double penalty problem encountered when computing skill scores for high-resolution forecast models (Mass et al., 2002). Mean and minimum heat index increase almost across the globe between both reference periods, with the most notable differences in minimum heat index over continents in the Northern Hemisphere.

An evaluation of the change in monthly mean heat index across the globe for both reference periods, as shown in Fig. 4, offers a glimpse into the temporal distribution of heat index changes in the course of the year. The monthly means of heat index clearly increase across the globe, most visibly around the equator during south winter and near the poles throughout the year.

ESSDD
8, 317–344, 2015

One of the most important applications of these data is the evaluation of danger due to high heat loads. We classified danger due to high heat index according to the criteria outlined in Table 1.

We computed heat index deciles globally for each reference period and used the classification criteria shown in Table 1 to find the probability that the peak heat index of each day would exceed the threshold for extreme danger in each month. Afterwards, we compared the exceedance likelihood between reference periods. The results, shown in Fig. 5, demonstrate that the likelihood of heat index values reaching levels that indicate "extreme danger" has increased worldwide in every month. South America during south summer and the Gulf of Mexico in north summer had especially large increases in likelihood of extreme danger.

3.2 Population-weighted heat index by country

As an example application of the new data set, countries were classified according to their heat index climatologies in each reference period. For both reference periods, 8 clusters were created from the monthly minima, means and maxima of population-weighted heat index in each country (see Fig. 6). This number of clusters matched both reference periods well – more clusters did not seem to produce any substantial gains, whereas less clusters would have meant a larger sum of squared distance between points inside individual clusters.

The clusters were examined using ordination plots based on the methods by Oksanen et al. (2014). As is shown in Fig. 7, the clusters created by the data for each reference period are similar, but not identical. The changes between both reference periods are shown more clearly in Fig. 8. Most changes are in Africa, southern Europe and Asia. A first visual analysis indicates that subtropical heat index climates have expanded away from the equator toward the poles. Especially cool, dry or humid areas retain their climatology across both reference periods.

ESSDD
8, 317–344, 2015

4 Conclusions

In this paper, we introduce a new data set containing gridded minimum, mean and maximum heat index values 2 m above ground for the entire globe for each day in the years 1979–2013. Due to the widespread use of heat index as an indicator for dangers to human health caused by heat loads, we believe that this data will be of great use in future studies concerning heat stress in the course of climate change. Our data set is new in the sense that it makes heat index values available on a high spatiotemporal resolution and on a spatially continuous grid for the entire planet. We show its potential for further studies by performing some initial, straightforward analyses that provide a first glimpse into the data.

It is shown that, for the two periods chosen for our study (1979–1999, 2000–2013), the distribution of heat index across the globe has changed. The worldwide mean heat index has risen, both for the entire year as well as for each month. The likelihood of daytime heat index values that indicate "extreme danger" has also increased across the globe since the 20th century. This analysis is meant as an example usage of this data and could be repeated for different thresholds, with a finer quantile resolution, or focused on more specific geographic areas or time periods in order to obtain more meaningful information.

It is also shown that, in the time period contained in the data set, many countries have transitioned from one heat index climate zone into another. As in the previous example, such country-level analyses are only one possible ways to use this data. Examining them on a finer spatiotemporal scale and combining them with additional data could reveal more information and aid in analyzing, understanding and predicting the connection between heat index and various components of human systems.

The data is available for general use (Lee, 2014) and the scientific community is encouraged to take advantage of it in studies evaluating heat index, its distribution through space and time, and its connections to and influence on human systems.

ESSDD
8, 317–344, 2015

The Supplement related to this article is available online at doi:10.5194/essdd-8-317-2015-supplement.

Acknowledgements. We thank the European Centre for Medium-Range Weather Forecasts for providing the original data. We also extend our thanks to all contributors to the several open source projects which were used in analyzing, manipulating and visualizing our data.

References

Alexander, L. V. and Arblaster, J. M.: Assessing trends in observed and modelled climate extremes over Australia in relation to future projections, Int. J. Climatol., 29, 417–435, doi:10.1002/joc.1730, 2009. 319

Anderson, G. B., Bell, M. L., and Peng, R. D.: Methods to calculate the heat index as an exposure metric in environmental health research, Environ. Health Persp., 121, 1111–1119, doi:10.1289/ehp.1206273, 2013. 320, 322, 327

Balk, D. and Yetman, G.: The global distribution of population: Evaluating the gains in resolution refinement, Tech. rep, Center for International Earth Science Information Network, Columbia University, Palisades, NY, available at: http://sedac.ciesin.columbia.edu/downloads/docs/gpw-v3/gpw3_documentation_final.pdf (last access: 13 March 2015), 2004. 325

Balk, D., Yetman, G., and Sherbinin, A. d.: Construction of gridded population and poverty data sets from different data sources, in: Proceedings of European Forum for Geostatistics Conference, European Forum for Geography and Statistics, Tallinn, Estonia, 12–20, available at: http://sedac.ciesin.columbia.edu/downloads/docs/gpw-v3/balk_etal_geostatpaper_2010pdf-1.pdf (last access: 13 March 2015), 2010. 324

Basara, J. B., Basara, H. G., Illston, B. G., and Crawford, K. C.: The impact of the urban heat island during an intense heat wave in Oklahoma City, Advances in Meteorology, 230365, 1–10, doi:10.1155/2010/230365, 2010. 320

ESSDD

8, 317–344, 2015

Beniston, M.: The 2003 heat wave in Europe: a shape of things to come? An analysis based on Swiss climatological data and model simulations, Geophys. Res. Lett., 31, L02202, doi:10.1029/2003GL018857, 2004. 319

Berrisford, P., Dee, D., Poli, P., Brugge, R., Fielding, K., Fuentes, M., Kållberg, P., Kobayashi, S., Uppala, S., and Simmons, A.: The ERA-Interim archive, version 2.0, Tech. Rep. 1, European Centre for Medium Range Weather Forecasts, Reading, available at: http://old.ecmwf.int/publications/library/ecpublications/_pdf/era/era_report_series/RS_1_v2.pdf (last access: 13 March 2015), 2009. 321

Bivand, R. and Rundel, C.: rgeos: Interface to Geometry Engine – Open Source (GEOS), available at: http://CRAN.R-project.org/package=rgeos (last access: 13 March 2015), r package version 0.3-8, 2014. 339, 340, 341

Burkart, K., Schneider, A., Breitner, S., Khan, M. H., Krämer, A., and Endlicher, W.: The effect of atmospheric thermal conditions and urban thermal pollution on all-cause and cardiovascular mortality in Bangladesh, Environ. Pollut., 159, 2035–2043, doi:10.1016/j.envpol.2011.02.005, 2011. 320

Calzadilla, A., Rehdanz, K., Betts, R., Falloon, P., Wiltshire, A., and Tol, R. S. J.: Climate change impacts on global agriculture, Tech. Rep. 1617, Kiel working paper, available at: http://www.econstor.eu/handle/10419/32519 (last access: 13 March 2015), 2010. 319

CIESIN (Center for International Earth Science Information Network) – Columbia University; IFPRI (International Food Policy Research Institute); The World Bank; CIAT (Centro Internacional de Agricultura Tropical): Gridded Population of the World (GPW), Version 3, available at: http://beta.sedac.ciesin.columbia.edu/gpw (last access: 13 March 2015), 2004. 324

CIESIN (Center for International Earth Science Information Network) – Columbia University; IFPRI (International Food Policy Research Institute); The World Bank; CIAT (Centro Internacional de Agricultura Tropical): Global Rural-Urban Mapping Project, Version 1 (GRUMPv1): Population Count Grid, doi:10.7927/H4VT1Q1H, 2011. 324

Dee, D. P., Uppala, S. M., Simmons, A. J., Berrisford, P., Poli, P., Kobayashi, S., Andrae, U., Balmaseda, M. A., Balsamo, G., Bauer, P., Bechtold, P., Beljaars, A. C. M., van de Berg, L., Bidlot, J., Bormann, N., Delsol, C., Dragani, R., Fuentes, M., Geer, A. J., Haimberger, L., Healy, S. B., Hersbach, H., Hólm, E. V., Isaksen, L., Kållberg, P., Köhler, M., Matricardi, M., McNally, A. P., Monge-Sanz, B. M., Morcrette, J.-J., Park, B.-K., Peubey, C., de Rosnay, P., Tavolato, C., Thépaut, J.-N., and Vitart, F.: The ERA-interim reanalysis: configuration and

ESSDD
8, 317–344, 2015

performance of the data assimilation system, Q. J. Roy. Meteor. Soc., 137, 553–597, doi:10.1002/qj.828, 2011. 321
Diffenbaugh, N. S. and Ashfaq, M.: Intensification of hot extremes in the United States: intensification of hot extremes, Geophys. Res. Lett., 37, L15701, doi:10.1029/2010GL043888, 2010. 319
Diffenbaugh, N. S. and Scherer, M.: Observational and model evidence of global emergence of permanent, unprecedented heat in the 20th and 21st centuries: a letter, Climatic Change, 107, 615–624, doi:10.1007/s10584-011-0112-y, 2011. 319
El Morjani, Z. E. A., Ebener, S., Boos, J., Abdel Ghaffar, E., and Musani, A.: Modelling the spatial distribution of five natural hazards in the context of the WHO/EMRO atlas of disaster risk as a step towards the reduction of the health impact related to disasters, Int. J. Health Geogr., 6, 8, doi:10.1186/1476-072X-6-8, 2007. 320
Everitt, B. and Hothorn, T.: A Handbook of Statistical Analyses Using R, CRC Press, Boca Raton, 2nd Edn., 2010. 326
GRASS Development Team: Geographic Resources Analysis Support System (GRASS GIS) Software, Open Source Geospatial Foundation, USA, available at: http://grass.osgeo.org (last access: 13 March 2015), 2012. 322
Hartigan, J. A. and Wong, M. A.: Algorithm AS 136: a K-means clustering algorithm, Applied Statistics, 28, 100–108, doi:10.2307/2346830, 1979. 326
Hijmans, R. J.: raster: Geographic data analysis and modeling, available at: http://CRAN.R-project.org/package=raster (last access: 13 March 2015), r package version 2.3-12, 2014. 324
International Organization for Standardization: Hot environments Estimation of the heat stress on working man, based on the WBGT-index (wet bulb globe temperature), Tech. Rep. 7423:1989, International Organization for Standardization, available at: http://www.iso.org/iso/catalogue_detail.htm?csnumber=13895 (last access: 13 March 2015), 2010. 320
IPCC (Intergovernmental Panel on Climate Change): Climate Change 2013 – The Physical Science Basis: Working Group I Contribution to the Fifth Assessment Report of the Intergovernmental Panel on Climate Change, Cambridge University Press, Cambridge, available at: http://ebooks.cambridge.org/ref/id/CBO9781107415324 (last access: 13 March 2015), 2014. 319

ESSDD
8, 317–344, 2015

Kjellstrom, T., Kovats, R. S., Lloyd, S. J., Holt, T., and Tol, R. S. J.: The direct impact of climate change on regional labor productivity, Arch. Environ. Occup. H., 64, 217–227, doi:10.1080/19338240903352776, 2009. 319

Kysely, J. and Kim, J.: Mortality during heat waves in South Korea, 1991 to 2005: how exceptional was the 1994 heat wave?, Clim. Res., 38, 105–116, doi:10.3354/cr00775, 2009. 320

Lawrence, M. G.: The relationship between relative humidity and the dewpoint temperature in moist air: a simple conversion and applications, B. Am. Meteorol. Soc., 86, 225–233, doi:10.1175/BAMS-86-2-225, 2005. 322

Lee, D.: Heat index at 2 m above ground: A globally gridded dataset based on reanalysis data from 1979–2013, links to GeoTIFFs, doi:10.1594/PANGAEA.841057, PANGEA, supplement to: D. Lee, "Perceived temperature in the course of climate change: An analysis of global heat index from 1979–2013", submitted, 2014. 320, 329

Mass, C. F., Ovens, D., Westrick, K., and Colle, B. A.: Does increasing horizontal resolution produce more skillful forecasts?, B. Am. Meteorol. Soc., 83, 407–430, doi:10.1175/1520-0477(2002)083<0407:DIHRPM>2.3.CO;2, 2002. 327

Meehl, G. A., Tebaldi, C., Walton, G., Easterling, D., and McDaniel, L.: Relative increase of record high maximum temperatures compared to record low minimum temperatures in the U.S., Geophys. Res. Lett., 36, L23701, doi:10.1029/2009GL040736, 2009. 319

Murphy, R.: Relative humidity, available at: http://www.erh.noaa.gov/bgm/tables/rh.shtml (last access: 13 March 2015), 2006. 322

National Institute for Occupational Safety and Health: Criteria for a Recommended Standard: Occupational Exposure to Hot Environments (Revised Criteria 1986), Tech. Rep. 86-113, National Institute for Occupational Safety and Health, available at: http://www.cdc.gov/niosh/docs/86-113/ (last access: 13 March 2015), 1986. 320

National Weather Service: Heat Index Equation, available at: http://www.hpc.ncep.noaa.gov/html/heatindex_equation.shtml (last access: 13 March 2015), 2014a. 322

National Weather Service: Heat Safety, available at: http://www.nws.noaa.gov/os/heat/index.shtml (last access: 13 March 2015), 2014b. 327, 336, 341

Oksanen, J., Blanchet, F. G., Kindt, R., Legendre, P., Minchin, P. R., O'Hara, R. B., Simpson, G. L., Solymos, P., Stevens, M. H. H., and Wagner, H.: vegan: Community Ecology Package, available at: http://CRAN.R-project.org/package=vegan (last access: 13 March 2015), r package version 2.2-0, 2014. 328

ESSDD
8, 317–344, 2015

Patterson, T. and Kelso, N. V.: Natural Earth, available at: naturalearthdata.com (last access: 13 March 2015), 2014. 325

Perry, A. G., Korenberg, M. J., Hall, G. G., and Moore, K. M.: Modeling and syndromic surveillance for estimating weather-induced heat-related illness, Journal of Environmental and Public Health, 2011, 1–10, doi:10.1155/2011/750236, 2011. 320

Poumadère, M., Mays, C., Le Mer, S., and Blong, R.: The 2003 heat wave in France: dangerous climate change here and now, Risk Anal., 25, 1483–1494, doi:10.1111/j.1539-6924.2005.00694.x, 2005. 319

R Core Team: R: A Language and Environment for Statistical Computing, R Foundation for Statistical Computing, Vienna, Austria, available at: http://www.R-project.org (last access: 13 March 2015), 2014. 324, 326

Rothfusz, L. P.: The Heat Index "Equation" (or, More Than You Ever Wanted To Know About Heat Index), Scientific Services Division, NWS Southern Region Headquarters, Fort Worth, Texas, available at: http://www.srh.noaa.gov/images/ffc/pdf/ta_htindex.pdf (last access: 13 March 2015), 1990. 322

Schär, C., Vidale, P. L., Lüthi, D., Frei, C., Häberli, C., Liniger, M. A., and Appenzeller, C.: The role of increasing temperature variability in European summer heatwaves, Nature, 427, 332–336, doi:10.1038/nature02300, 2004. 319

Sherwood, S. C., Meyer, C. L., Allen, R. J., and Titchner, H. A.: Robust tropospheric warming revealed by iteratively homogenized radiosonde data, J. Climate, 21, 5336–5352, doi:10.1175/2008JCLI2320.1, 2008. 319

Smith, T. M., Peterson, T. C., Lawrimore, J. H., and Reynolds, R. W.: New surface temperature analyses for climate monitoring: surface temperature analyses, Geophys. Res. Lett., 32, L14712, doi:10.1029/2005GL023402, 2005. 319

South, A.: rworldmap: A New R package for Mapping Global Data, The R Journal, 3, 35–43, available at: http://journal.r-project.org/archive/2011-1/RJournal_2011-1_South.pdf (last access: 13 March 2015), 2011. 339, 340, 341

Steadman, R. G.: The assessment of sultriness. Part II: Effects of wind, extra radiation and barometric pressure on apparent temperature, J. Appl. Meteorol., 18, 874–885, doi:10.1175/1520-0450(1979)018<0874:TAOSPI>2.0.CO;2, 1979. 322

Thorne, P. W. and Vose, R. S.: Reanalyses suitable for characterizing long-term trends: are they really achievable?, B. Am. Meteorol. Soc., 91, 353–361, doi:10.1175/2009BAMS2858.1, 2010. 321

ESSDD
8, 317–344, 2015

Vose, R. S., Wuertz, D., Peterson, T. C., and Jones, P. D.: An intercomparison of trends in surface air temperature analyses at the global, hemispheric, and grid-box scale: intercomparison of temperature analyses, Geophys. Res. Lett., 32, L18718, doi:10.1029/2005GL023502, 2005. 319

Wickham, H.: ggplot2: Elegant Graphics for Data Analysis, Springer, New York, available at: http://had.co.nz/ggplot2/book (last access: 13 March 2015), 2009. 326

ESSDD

8, 317–344, 2015

Table 1. Heat index danger levels according to National Weather Service (2014b).

°F	Danger level
> 80	Caution
> 91	Extreme caution
> 103.5	Danger
> 126	Extreme danger

ESSDD
8, 317–344, 2015

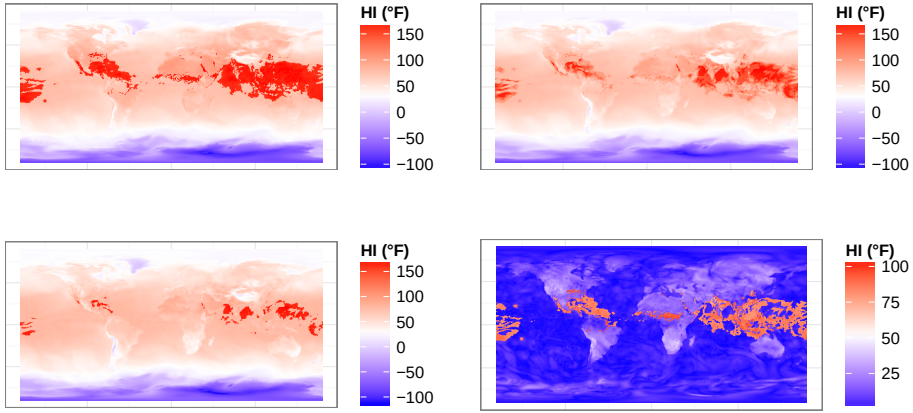

Figure 1. Typical heat index for an exemplary day (2 June 1996). Counterclockwise from the top left corner: maximum heat index; minimum heat index; mean heat index; diurnal cycle of heat index.

ESSDD
8, 317–344, 2015

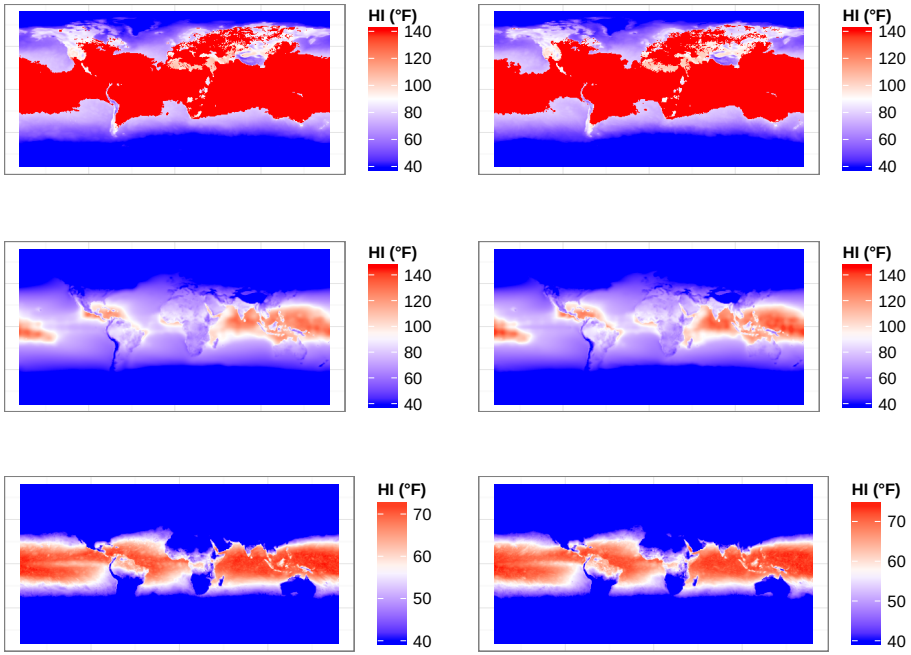

Figure 2. Yearly temporal statistics of heat index for each reference period (1979–1999, 2000–2013). The left column is the first reference period, the right column the second. The rows are, from top to bottom, the yearly maximum, mean and minimum.

ESSDD
8, 317–344, 2015

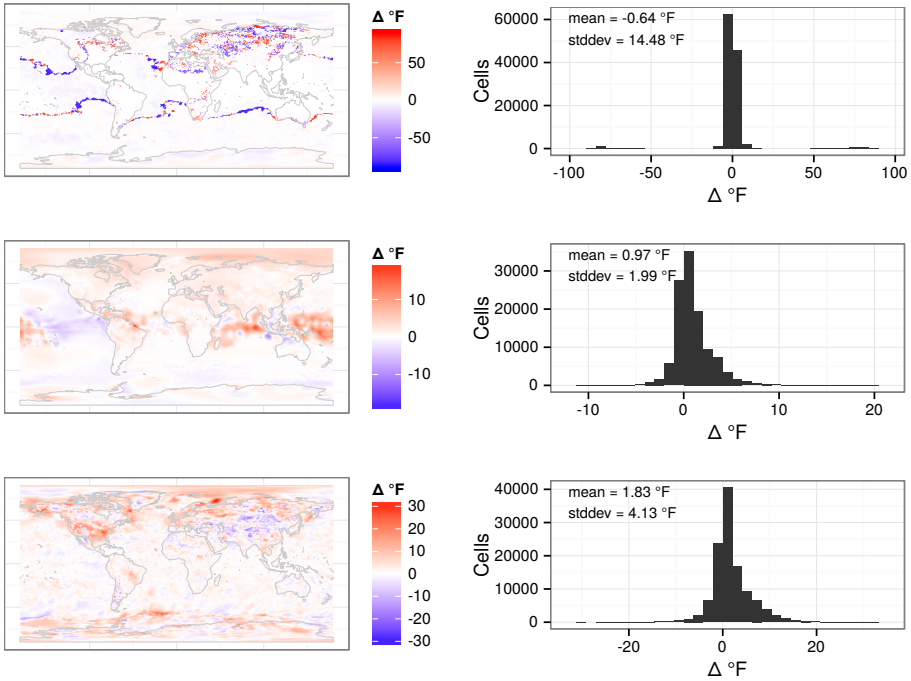

Figure 3. Differences between yearly temporal statistics of heat index for each reference period (1979–1999, 2000–2013). The left column shows, from top to bottom, the differences in maximum, mean and minimum heat index for the entire year for the entire globe. The right column shows the frequencies of heat index changes worldwide in number of cells, with the mean change in heat index and standard deviance noted in the plot. Continents are added for orientation (South, 2011; Bivand and Rundel, 2014).

ESSDD
8, 317–344, 2015

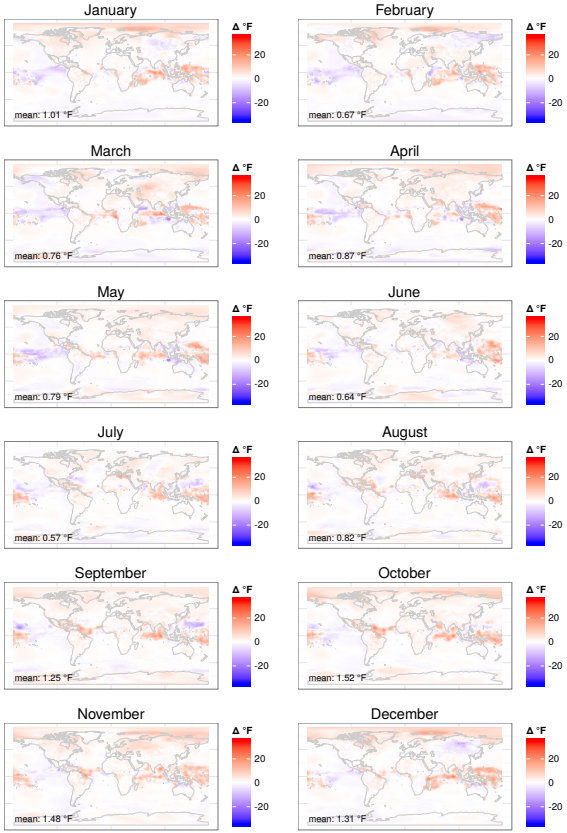

Figure 4. Differences between both reference periods (1979–1999, 2000–2013) in monthly mean heat index. Continents are added for orientation (South, 2011; Bivand and Rundel, 2014).

ESSDD
8, 317–344, 2015

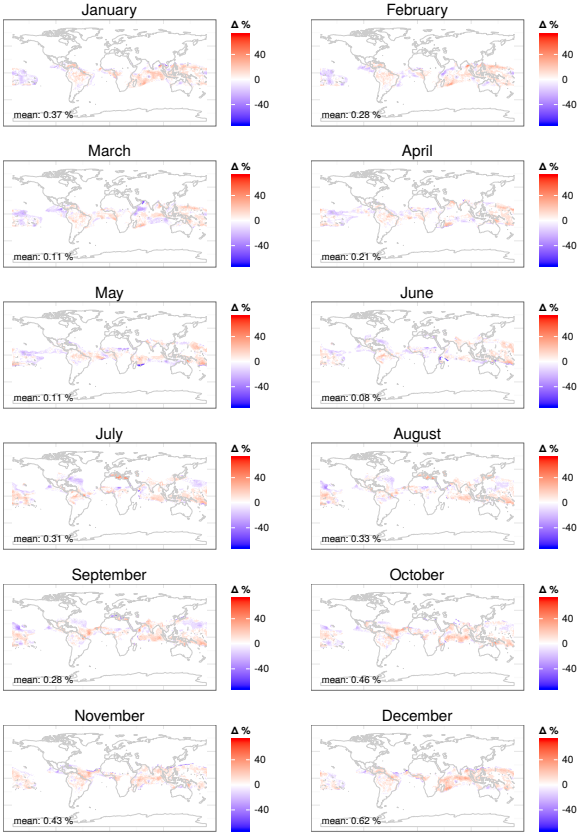

Figure 5. Changes in the probability that the peak temperature will exceed the threshold for "extreme danger" for a given day in each month in both reference periods (National Weather Service, 2014b). Continents are added for orientation (South, 2011; Bivand and Rundel, 2014).

ESSDD
8, 317–344, 2015

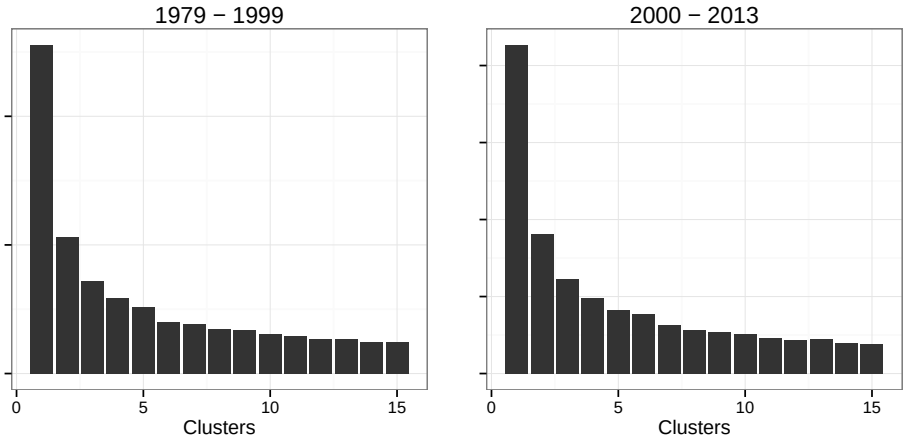

Figure 6. Sum of squared distance between points for various numbers of clusters when grouping countries by population-weighted heat index minima, means and maxima in each month in both reference periods.

ESSDD
8, 317–344, 2015

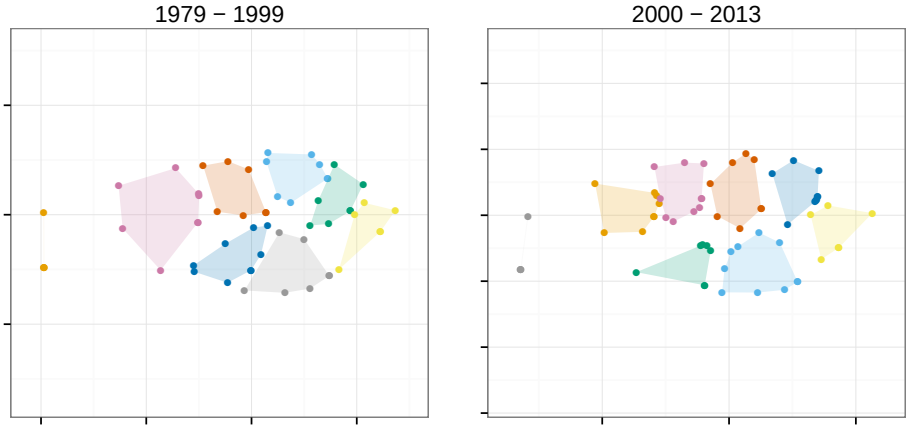

Figure 7. Ordination plot of clusters of countries based on their monthly minimum, mean and maximum heat index values for each month in each reference period. A total of 8 clusters were identified.

ESSDD
8, 317–344, 2015

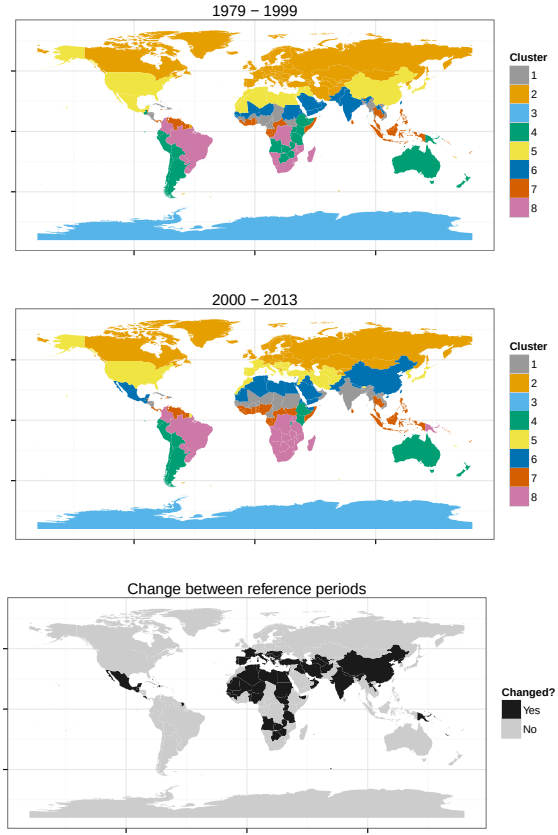

Figure 8. Countries and the clusters they were grouped into. The map at the top shows country clusters for the first, the map in the middle county clusters for the second reference period. The map at the bottom indicates whether a country was grouped into different clusters between both periods.

ESSDD
8, 317–344, 2015